Cationic State Distribution over the P700 Chlorophyll Pair in Photosystem I.

AUTHOR(S):

Saito, Keisuke; Ishikita, Hiroshi

CITATION:

Saito, Keisuke ...[et al]. Cationic State Distribution over the P700 Chlorophyll Pair in Photosystem I.. Biophysical journal 2011, 101(8): 2018-2025

ISSUE DATE:

2011-10-19

URL:

http://hdl.handle.net/2433/150116

Cationic state distribution over the P700 chlorophyll pair in Photosystem I

Keisuke Saito[†], and Hiroshi Ishikita[†‡*]

[†]Career-Path Promotion Unit for Young Life Scientists, Kyoto University, 202 Building E, Graduate School of Medicine, Yoshida-Konoe-cho, Sakyo-ku, Kyoto 606-8501, Japan

[‡]Japan Science and Technology Agency (JST), PRESTO, 4-1-8 Honcho Kawaguchi, Saitama 332-0012, Japan

Running title: P700 charge state in Photosystem I

*correspondence to: H. Ishikita, Career-Path Promotion Unit for Young Life Scientists, Kyoto University, 202 Building E, Graduate School of Medicine, Yoshida-Konoe-cho, Sakyo-ku, Kyoto 606-8501, Japan (E-mail: hiro@cp.kyoto-u.ac.jp, TEL: +81-75-753-9286, FAX: +81-75-753-9281)

Keywords Photosystem I, P700, chlorophyll, spin density distribution, charge delocalization, electron transfer

The primary electron donor P700 in photosystem I is composed of two chlorophylls P_A and P_B. P700 forms the cationic $[P_A/P_B]^{\bullet+}$ state as a result of light-induced electron transfer. We obtained a $P_A^{\bullet+}/P_B^{\bullet+}$ ratio of 28/72 and a spin distribution of 22/78 for the entire PSI protein–pigment complex. By considering the influence of the protein components on the redox potential for one-electron oxidation of P_A/P_B monomers, we found that the following three factors significantly contributed to a large $P_B^{\bullet+}$ population relative to $P_A^{\bullet+}$: (i) Thr-A743 forming a H-bond with P_A, (ii) P_A as a chlorophyll *a* epimer, and (iii) a conserved PsaA/PsaB pair, the Arg-A750/Ser-B734 residue. In addition, (iv) the methyl-ester groups of the accessory chlorophylls A_{-1A}/A_{-1B} significantly stabilized the cationic $[P_A/P_B]^{\bullet+}$ state and (v) the methyl-ester group orientations were completely different in A_{-1A} and A_{-1B} as seen in the crystal structure. When the methyl-ester group was rotated, the spin-density distribution over P_A/P_B ranged from 22/78 to 15/85.

In oxygenic photosynthesis, photosystem I (PSI) participates in the conversion of light to chemical energy with photosystem II (PSII). Light-induced electron transfer occurs along a series of cofactors bound to the PsaA and PsaB subunits of PSI. On the lumen side, there exists a chlorophyll dimer P700 composed of two chlorophylls P_A and P_B. P_B is chlorophyll *a* (Chl*a*) and P_A is Chl*a*′, the $C13^2$ epimer of Chl*a* (Figure 1a) (*1; 2*). A second Chl*a* pair next to P_A/P_B is the accessory Chl*a* A_{-1A}/A_{-1B}. In addition, there are two additional distant Chl*a* (A_0), two phylloquinones (A_1), and one iron–sulfur cluster (F_X) in the PsaA/PsaB subunits. Similar to PSII, these six Chl*a* and two phylloquinones are arranged in two electron-transfer branches (A and B), which adopt a pseudo-C_2 symmetry with the rotation axis passing through P_A/P_B and F_X. In PSII, only one of the two branches serves as an electron-transfer active branch; this is in contrast to PSI, in which two branches are electron-transfer active (*3*), as shown by the biphasic forward electron transfers from P700 to A_1 or from A_1 to F_X observed in kinetic studies.

The primary process of charge separation culminates with a hole on the P_A/P_B pair in PSI or on the P_{D1}/P_{D2} pair in PSII. In PSII, the cationic state over P_{D1}/P_{D2} is predominantly observed in the Chl*a* of the electron active branch P_{D1}, with a $P_{D1}^{\bullet+}/P_{D2}^{\bullet+}$ ratio of ~80/20 (*4; 5*). For PSI, the $P_A^{\bullet+}/P_B^{\bullet+}$ ratios or the corresponding spin-density distributions were obtained experimentally by Fourier transform infrared (FTIR) spectroscopy (*6*) or electron paramagnetic resonance (EPR) (*4; 7; 8*) studies, respectively. FTIR studies indicated that the $P_A^{\bullet+}/P_B^{\bullet+}$ ratios were in the range of 50/50 to 33/67 (*6*). On the other hand, the spin-density distribution over P_A/P_B is 25/75 (*4*) and 25/75–20/80 in PSI from spinach (*7*) and 15/85 in PSI from *T. elongatus* (*8*) (reviewed in Ref. (*9*)).

To understand the role of the amino acid residues or cofactors of PSI in the energetics of P700, influences of all amino acid residues and redox active cofactors on the energetics of P_A/ P_B Chl*a* monomers as well as the P700 Chl*a* dimer are first time elucidated. We present the following: (i) The computational results of the influence of the PSI protein environment on the redox potentials, $E_m(P_A)$ and $E_m(P_B)$, are presented on the basis of the PSI crystal structure (*2*) in the presence of all protein subunits and cofactors. The linear Poisson–Boltzmann equation is solved by considering the

protonation states of all titratable sites in PSI. (ii) The $P_A^{\bullet+}/P_B^{\bullet+}$ ratio for the P_A/P_B pair is calculated using a large-scale quantum chemical/molecular mechanical (QM/MM) approach with explicit treatment of the complete PSI atomic coordinates divided into two subsystems; the QM region contains the P_A/P_B dimer and is treated by quantum mechanics (unrestricted DFT/B3LYP and LACVP* level) and the remaining protein subunits and cofactors are treated with the MM force field. The computational conditions and procedures used in studies on the *T. vulcanus* PSII (*10*) (using the 1.9-Å structure (*11*)) were consistently used in the present study; this can facilitate the direct analysis and comparison of the influences of protein environments on Chl*a* in both PSI and PSII.

EXPERIMENTAL PROCEDURES

In this article, we employed the following systematic modeling procedure. First, we constructed a realistic molecular model of the whole PSI protein–pigment complex using a high-resolution crystal structure. On the basis of this atomistic model, we evaluated the redox potential of P_A/P_B by solving the linear Poisson–Boltzmann equation with explicit consideration of the protonation states for all titratable residues. Second, to gain deeper insights into the electronic structure of P_A/P_B Chl*a*′/Chl*a* heterodimer, we performed large-scale QM/MM calculations for the entire PSI protein–pigment complex. Finally, after confirming the validity of the computational results through comparison with available experimental data, we discussed the atomistic origin that determines the asymmetric distribution of the cationic state of the P_A/P_B pair. Technical details of each modeling procedure are summarized as follows.

Coordinates. The atomic coordinates were taken from the X-ray structure of the PSI protein–pigment complex from *T. elongatus* at 2.5 Å resolution (protein data bank code: 1JB0) (*11*). Hydrogen atoms were generated and energetically optimized using the CHARMM force field (*12*). The positions of all non-hydrogen atoms were fixed, and all titratable groups were kept in their standard protonation states; i.e., acidic groups were ionized and basic groups were protonated. For the QM/MM calculations, we added additional counter ions to neutralize the whole system.

Atomic partial charges. Atomic partial charges of the amino acids were adopted from the all-atom CHARMM22 (*13*) parameter set. The charges of the protonated acidic O atoms were increased successively by +0.5 units to implicitly account for the presence of a proton. Similarly, instead of removing a proton to generate the deprotonated state, the charges of all of the protons of the basic groups of Arg and Lys were successively diminished to a total of one unit of charge. For residues for which the protonation states were not available in the CHARMM22 parameter set, appropriate charges were computed (*14*). For the atomic charges of Chl*a* (except for P_A/P_B) and quinones, we used atomic partial charges from previous studies on PSI (*15-17*); the charges were determined by fitting the surrounding electrostatic potential of these molecules using the RESP procedure (*18*). The charges of equivalent H atoms (e.g., three H atoms of methyl group) were averaged. The electronic wave functions were calculated after geometry optimization with the DFT module in JAGUAR (*19*) (B3LYP/LACVP*) (Table S1 in the Supporting Information).

Computation of redox potential E_m(Chl*a*). The present computation was based on the electrostatic continuum model, where the linear Poisson–Boltzmann equation was solved using the

MEAD program (*20*). To facilitate direct comparisons with previous computational results, identical computational conditions and parameters such as atomic partial charges and dielectric constants were used (*21; 22*). The redox states of all other cofactors (e.g., A_{-1} and A_0 Chl*a*, and A_1 quinone) were kept in their neutral charge states during the redox titration of each Chl*a*. We considered F_X, F_A, and F_B in the oxidized charge state $[Fe_4S_4(SCH_3)_4]^{2-}$ for the wild-type PSI as in previous studies (*15-17*). The ensemble of the protonation patterns was sampled using the Monte-Carlo method with the Karlsberg program (Rabenstein, B. *Karlsberg online manual*, http://agknapp.chemie.fu-berlin.de/karlsberg/ (1999)) (*23*). The dielectric constants were set to $\varepsilon_p = 4$ inside the protein and $\varepsilon_w = 80$ for water. All computations were performed at 300 K, pH 7.0, and an ionic strength of 100 mM. The linear Poisson–Boltzmann equation was solved using a three-step grid-focusing procedure at resolutions of 2.5, 1.0, and 0.3 Å. The Monte-Carlo sampling for a redox active group yielded the probabilities $[A_{ox}]$ and $[A_{red}]$ of the two redox states of molecule A. The shifts in E_m(Chl*a*′) and E_m(Chl*a*) due to the PSI protein environment were evaluated using the Nernst equation. A bias potential was applied to obtain an equal amount of both redox states ($[A_{ox}] = [A_{red}]$), yielding the redox midpoint potential E_m as the resulting bias potential. For convenience, the computed E_m was represented in millivolt accuracy and the last digit was not considered to be significant.

QM/MM calculations. In all QM/MM calculations reported here, we employed the so-called electrostatic embedding QM/MM scheme. In all the QM/MM calculations, we used the Qsite (*24*) program code. The electrostatic and steric effects created because of the complex PSI architecture were explicitly considered in all calculations. Owing to the large system size of PSI, the QM region was limited to the P_A/P_B Chl*a*′/Chl*a* heterodimer for simplicity, while the other protein units and all co-factors were approximated by the MM force field. Because the atomic partial charges were optimized (e.g., A_{-1} and A_0 Chl*a*, and A_1 quinone), the QM/MM partition was accurate enough to describe the electronic structure of the $[P_A/P_B]^{\bullet+}$ Chl*a*′/Chl*a* heterodimer. To reliably determine the cationic character of the $[P_A/P_B]^{\bullet+}$ heterodimer, we employed the unrestricted DFT method with the B3LYP functional and LACVP* basis sets. The $[P_A/P_B]^{\bullet+}$ heterodimer geometry was refined by the constrained QM/MM optimizations; for the surrounding MM protein environment, the atomistic coordinates were exactly fixed with the original X-ray coordinates. After obtaining the stable geometry of the QM fragment, we determined the ESP charges for the cationic state of the $[P_A/P_B]^{\bullet+}$ heterodimer in the presence of the entire PSI atomic coordinates (Table S1 in the Supporting Information).

RESULTS AND DISCUSSION

$P_A^{\bullet+}/P_B^{\bullet+}$ ratio and spin-density distribution in wild-type PSI. The $P_A^{\bullet+}/P_B^{\bullet+}$ ratio was calculated to be 27.9/72.1 (Table 1a), demonstrating that the cationic state is stabilized more in P_B than in P_A: this should result in the value of $E_m(P_B)$ being lower than that of $E_m(P_A)$. The $P_A^{\bullet+}/P_B^{\bullet+}$ ratio of 27.9/72.1 was considerably close to the charge-distribution ratio of 33/67 obtained from FTIR studies of PSI from *Synechocystis* sp. PCC 6803 (*6*). The calculated spin-density distribution over P_A/P_B was 22.4/77.6 (Table 1a), which shows greater asymmetry than the ratio of the charge

distribution (i.e., $P_A^{\bullet+}/P_B^{\bullet+}$), a fact already pointed out previously in PSII (*25; 26*). The obtained value was in good agreement with the experimental values of 25/75 (*4*) and 25/75–20/80 of PSI from spinach (*7*) and 15/85 of PSI from *T. elongatus* (*8*) (note: according to another interpretation of the *T. elongatus* data (*8*), the ratio of 25/75 to 30/70 may be possible (*9*)).

The PSI protein environment shifted the E_m values of P_A/P_B only marginally from those of the reference model system (Table 1a). The shifts were essentially the same for P_A and P_B. However, the resulting E_m values for the P_A/P_B molecules must be different because of the difference between E_m(Chl*a*′) and E_m(Chl*a*) in the reference model system. Although the difference between E_m(Chl*a*′) and E_m(Chl*a*) is not known so far, we infer that the former may be higher than the latter because Chl*a*′ is thermodynamically less stable than Chl*a* (Figure 1b) (*9*).

Influence of H-bond on the $P_A^{\bullet+}/P_B^{\bullet+}$ ratio. The -OH group of Thr-A743 can form a H-bond with the 13^1-keto group of P_A, whereas the corresponding H-bond is absent in P_B. A mutation of Thr-A743 to Val would result in the loss of the H-bond (*27; 28*). Using the wild-type PSI crystal structure, we modeled the T(A743)V PSI by substituting the -OH side chain group of Thr with $–CH_3$ (followed by geometry optimization of the A743 side chain while all of the other parts remained fixed).

$E_m(P_A)$ was lowered by ~10 mV upon the T(A743)V mutation while $E_m(P_B)$ remained unchanged (Table 1a). The marginal downshift in $E_m(P_A)$ was in agreement with a relatively weak H-bond of Thr-A743, as pointed out in spectroscopic studies (*29*). As $E_m(P_A)$ was lowered (i.e., $P_A^{\bullet+}$ was stabilized), the calculated $P_A^{\bullet+}/P_B^{\bullet+}$ ratio was significantly shifted and the population of $P_A^{\bullet+}$ increased from 27.9 in the wild-type PSI to 32.2 in the T(A743)V PSI (Table 1a). This observed $P_A^{\bullet+}$ population shift is in agreement with (i) the previous proposal that deletion of the H-bond leads to a downshift in $E_m(P_A)$ (*27*) and (ii) the experimentally observed relocation of ~14–18 % of the cationic state from P_B to P_A upon T(A743)V mutation in PSI from *Chlamydomonas reinhardtii* (*28*). The slightly smaller relocation of the cationic state (i.e., an increase in $P_A^{\bullet+}$ by 5%) in the present study is possibly due to (i) the difference between the used T(A743)V PSI model structure where the -OH group of Thr was replaced with $–CH_3$, without altering the other parts of the atomic coordinates (to avoid an uncertainty of prediction of the protein structure), or (ii) the difference of the PSI proteins between *T. elongatus* PSI (corresponds to the crystal structure (*2*)) and the *Chlamydomonas reinhardtii* PSI. As E_m(P700) differs by up to ~70 mV among different species (*30*), the P_A/P_B moiety may be slightly different among different species.

The individual values of $E_m(P_A)$ and $E_m(P_B)$ are not known experimentally due to the presence of their coupling. It is particularly difficult to determine $E_m(P_A)$ because of the small amount of $P_A^{\bullet+}$ compared with $P_B^{\bullet+}$. The present study demonstrates that shifts in $E_m(P_A)$ alter the distribution of the cationic (spin) state over P_A/P_B as reported in mutational studies (*27; 28*).

Influence of $C13^2$ epimer Chl*a*′ on $P_A^{\bullet+}/P_B^{\bullet+}$ ratio. The asymmetric charge distribution over P_A/P_B may also result from the asymmetry of the molecular geometry in P_A/P_B. The methyl-ester (CH_3COO-) groups in Chl*a*′ and Chl*a* are oppositely orientated with respect to the chlorin plane. Except for this methyl-ester orientation difference, the molecular structures of P_A and P_B are

essentially identical (*2*).

To investigate this orientation difference on the $P_A^{\bullet+}/P_B^{\bullet+}$ ratio, it would have been more relevant to replace Chl*a*′ of P_A with Chl*a*. Unfortunately, a replacement of Chl*a*′ of P_A with Chl*a* leads to unreasonable contacts with Tyr-A603, Gly-A739, Thr-A742, and Thr-A743. As an alternative, we substituted the CH_3COO- groups with H in both P_A and P_B (deletion of CH_3COO-), and calculated the $P_A^{\bullet+}/P_B^{\bullet+}$ ratio. Upon deletion of the CH_3COO- groups the $P_A^{\bullet+}$ population increases by ~5 % relative to the wild-type PSI, resulting in a $P_A^{\bullet+}/P_B^{\bullet+}$ ratio of 32.2/67.8 (Table 1a). Thus, the orientation difference in Chl*a*′/Chl*a* significantly influences the $P_A^{\bullet+}/P_B^{\bullet+}$ ratio in the PSI protein environment.

Under vacuum conditions, the P_A/P_B heterodimer yielded a $P_A^{\bullet+}/P_B^{\bullet+}$ ratio of 41.5/58.5 (Table 1b), which indicates a considerably delocalized cationic state distribution over P_A/P_B in the absence of the PSI protein environment. The deletion of CH_3COO- from P_A/P_B delocalized the cationic state giving a $P_A^{\bullet+}/P_B^{\bullet+}$ ratio of 45.5/54.5 (Table 1b); i.e., the cationic state is almost equally distributed over P_A/P_B. It can be concluded that in the absence of the PSI protein environment, the orientation of the CH_3COO- group in P_A is predominantly responsible for the $P_A^{\bullet+}/P_B^{\bullet+}$ ratio.

Influence of PsaA/PsaB symmetrical residue pairs on the $P_A^{\bullet+}/P_B^{\bullet+}$ ratio. The protein environment, in particular the charged residues, contribute to E_m shifts of the redox active site significantly. Because the E_m difference $E_m(P_A) - E_m(P_B)$ (= ΔE_m) is a key factor that can alter the $P_A^{\bullet+}/P_B^{\bullet+}$ ratio (*27*) (Figure 2), it is important to clarify the contributions of residues, in particular those located in the PsaA/PsaB heterodimer subunits.

Arg-A750, located on the lumenal side (Figure 3a), upshifted $E_m(P_A)$ the most by 65 mV, due to its positively charged protonated state (Table 2a). The Arg-A651 on the lumen side and Arg-A728 near F_X, both upshifted $E_m(P_A)$ by 35 mV. Arg-A728 is ~20 Å away from P_A/P_B, but its electrostatic influence on $E_m(P_A)$ and $E_m(P_B)$ is significant because of the complete absence of other titratable residues in the region between P_A/P_B and F_X (Figure 3d).

As both Arg-A651 and Arg-A728 concomitantly increase $E_m(P_A)$ and $E_m(P_B)$ with almost same magnitude (Table 2a), these residues were not responsible for the asymmetric distribution of $P_A^{\bullet+}/P_B^{\bullet+}$. Furthermore, according to the protein sequence alignment (with the CLUSTAL program (*31*)), Arg-A651 and Arg-A728 in PsaA are conserved as Arg-B627 and Arg-B712 in PsaB, respectively, which also upshifts $E_m(P_A)$ and $E_m(P_B)$ (Table 2a).

The same argument also holds true for the E_m downshifting residues, which are mainly acidic residues (Table 2b). Asp-B444 significantly downshifted $E_m(P_A)$ by 90 mV and $E_m(P_B)$ by 63 mV; and its counterpart in PsaA, Asp-A463, downshifted $E_m(P_A)$ by 67 mV and $E_m(P_B)$ by 98 mV. Thus, the influence of Asp-B444 on ΔE_m is completely compensated for by the influence of the counterpart Asp-A463.

To clarify how the PSI protein environment differentiates $P_A^{\bullet+}/P_B^{\bullet+}$, it is not sufficient to search for the residue that induces large changes in E_m values, instead it is important to find a “residue pair of PsaA/PsaB” that increases ΔE_m (Figure 2). Bearing this in mind, we found only a few residue pairs that contribute to non-zero values of ΔE_m. The residue pair, Arg-A750/Ser-B734, increased

ΔE_m by 17 mV (Table 3a). Note that the residue pair is fully conserved in cyanobacteria and green plants (Figure 4). The Arg-A750/Ser-B734 pair is located near P_A/P_B on the lumen side (Figure 3c). Indeed, Arg-A750 was already mentioned as the residue that upshifted $E_m(P_A)$ the most among all residues in PSI (Table 2) while its counterpart is an uncharged residue, Ser.

In the absence of the atomic charges of Arg-A750/Ser-B734, we obtained the $P_A^{\bullet+}/P_B^{\bullet+}$ ratio of 30.6/69.4; in which the $P_A^{\bullet+}$ population has increased by ~3 %, with respect to wild-type PSI (Table 1). This result indicates that, in turn the Arg-A750/Ser-B734 pair contributes to increase the $P_B^{\bullet+}$ population in the wild-type PSI by increasing ΔE_m.

The Arg-A750/Ser-B734 residue pair contributes the most to ΔE_m among all PsaA/PsaB residue pairs, however it increases ΔE_m only by 17 mV (Table 3a). The second most contributing residue pair —/Asp-B92, in which the corresponding residue in PsaA is absent among cyanobacteria and green plants (Figure 4), contributes 9 mV to ΔE_m (Table 3a). Hence, in comparison with the much larger influence of a number of D1/D2 residue pairs on the $E_m(P_{D1})/E_m(P_{D2})$ difference in PSII (*10*), the protein environments of PsaA and PsaB in PSI are quite similar in their electrostatic characters.

The residue pairs Arg-A750/Ser-B734 and —/Asp-B92 are responsible for ΔE_m in wild-type PSI. Mutations of these residues would produce other protonation patterns of the titratable residues of PSI to compensate for the induced changes (e.g., charges or protein conformations). Unless the protonation pattern of the titratable residues and the protein conformation remain unchanged upon the corresponding mutations, mutational studies do not directly correspond to the present results of the wild-type PSI.

Differences in the two accessory Chl*a* pairs A_{-1A} and A_{-1B}. There are also pairs that contribute to decrease ΔE_m and facilitate an accumulation of $P_B^{\bullet+}$. Unexpectedly, the most influential was the accessory Chl*a* pair, A_{-1A} and A_{-1B}, which decreased ΔE_m by 28 mV (Table 3b). It was surprising, because both A_{-1A} and A_{-1B} are identical molecules, Chl*a*, and the methyl-ester groups of P_A/P_B, i.e., the region causing the Chl*a*′/Chl*a* difference, is sufficiently far from the interface between P_A/P_B and A_{-1A}/A_{-1B}.

As expected from the ΔE_m value, eliminating the atomic charges of A_{-1A} and A_{-1B} resulted in the decrease in the $P_A^{\bullet+}$ population, shifting the $P_A^{\bullet+}/P_B^{\bullet+}$ ratio to 24.0/76.0 (Table 1). Thus, the influence of the accessory Chl*a* pair on the $P_A^{\bullet+}/P_B^{\bullet+}$ ratio as well as ΔE_m appears to be significant.

We first time found that the difference in the energy contribution of A_{-1A}/A_{-1B} to P_A/P_B results from the orientation of the methyl-ester groups of A_{-1A}/A_{-1B}, which are orientated at an angle of ~180° to each other across the $C13^2$-$C13^3$ axis (Figure 5). Because the methyl-ester groups are situated on the same side of the chlorin plane, the A_{-1A}/A_{-1B} pair consist of methyl-ester rotamers and not methyl-ester epimers. The carbonyl O atom of A_{-1A} is 5.4 Å away from the Mg atom of P_A whereas the corresponding distance is 7.1 Å between A_{-1B} and P_B (Figure 5). Because the carbonyl O atom is polarized more than the ester O atom, the methyl-ester group of A_{-1A} can stabilize the cationic $P_A^{\bullet+}$ state more effectively than that of the A_{-1B} for the $P_B^{\bullet+}$ state, thus decreasing $E_m(P_A)$ relative to $E_m(P_B)$. The possible role of the methyl-ester orientation of a Chl*a* in altering the E_m of another Chl*a* in the neighborhood was originally reported in PSII (*32*), and the present results

indicate that the same phenomenon holds true for P_A/P_B in PSI. Note that a clear discrimination between the –O–CH_3 and O edges of the ester-group in the electron density map was possible at a resolution of ~2.5 Å (W. Saenger, personal communications).

The H-bonding partner or any groups that specifies the orientation of the methyl-ester groups of A_{-1A}/A_{-1B} or case steric hindrance is absent. By rotating each methyl-ester group in A_{-1A}/A_{-1B} is rotated by 180° along the $C13^2$–$C13^3$ axis, the $P_A^{\bullet+}/P_B^{\bullet+}$ ratio changed from 27.9/72.1 (wild type) to 22.4/77.6 (rotated methyl-ester: A_{-1A}/A_{-1B}, Table 4) and the corresponding spin-density distributions in P_A/P_B were shifted from 22.4/77.6 to 15.1/84.9, respectively. The spin-density distribution of 15.1/84.9 was considerably shifted from the wild-type PSI value. A similar value of the spin-density distribution (15/85) was reported from EPR studies of PSI from *T. elongatus* (*8*). As the energy required for rotation of the methyl-ester group is not unusually large (due to the sp^3 carbons) and the H-bonding partner that specifies the orientation of the methyl-ester groups of A_{-1A}/A_{-1B} is absent, it is reasonable to assume that the $P_A^{\bullet+}/P_B^{\bullet+}$ ratio and the spin-density distribution over P_A/P_B fluctuates within the ranges given in Table 4. Hence, the orientation of the methyl-ester group in A_{-1A}/A_{-1B} can affect the P_A/P_B ΔE_m and the $P_A^{\bullet+}/P_B^{\bullet+}$ ratio.

CONCLUSIONS

The $P_A^{\bullet+}/P_B^{\bullet+}$ ratio of the P_A/P_B dimer calculated over the entire PSI protein was 28/72, which was close to the charge-distribution ratio of 33/67 obtained in the FTIR studies of PSI from *Synechocystis* sp. PCC 6803 (*6*). The calculated spin density, which was asymmetrically distributed over the P_A/P_B dimer with a ratio of 22/78, was in good agreement with the experimental values of 25/75 (*4*) and 20/80 in EPR studies from spinach (*7*). The Chl*a*′/Chl*a* difference for P_A/P_B was revealed to be partially responsible for the larger population of the $P_B^{\bullet+}$ state, from the methyl-ester deletion simulations. Removal of the H-bond between P_A and Thr-A743 in T(A743)V mutation, resulted in a slight decrease in $E_m(P_A)$ and a partial movement of the cationic state from P_A to P_B, as suggested by mutational studies (*27; 28*).

Conserved PsaA/PsaB pairs, Arg-A651/Arg-B627 and Arg-A728/Arg-B712 upshifted both $E_m(P_A)$ and $E_m(P_B)$ by ~30 mV, and Asp-A463/Asp-B444 and Asp-A593/Asp-B580 residue pairs downshifted both $E_m(P_A)$ and $E_m(P_B)$ in the range ~30–60 mV. The residue pair that led to a notable value of ΔE_m (i.e., $E_m(P_A) > E_m(P_B)$) was Arg-A750/Ser-B734, with a ΔE_m of 17 mV, thus contributing to an increase in the $P_B^{\bullet+}$ population (Note that a simple mutation of the residues would cause a change in the protonation states of the titratable residues in PSI, compensating for changes in the net charges of the mutated sites.). On the other hand, the most influential pair enhancing $E_m(P_A) < E_m(P_B)$ was the accessory A_{-1A}/A_{-1B} Chl*a* pair, with a ΔE_m of 28 mV; this pair contributed to an increase in the $P_A^{\bullet+}$ population in the original PSI crystal structure. The different influence of A_{-1A} and A_{-1B} on $E_m(P_A)$ and $E_m(P_B)$ was due to the differences in their methyl-ester orientations. Rotation of the methyl-ester groups alters the P_A/P_B spin-density distributions from 22/78 to 15/85. The latter value was in agreement with the value of 15/85 measured by EPR for PSI from *T. elongatus* (*8*).

REFERENCES

1. Watanabe T., M. Kobayashi, A. Hongu, M. Nakazato, T. Hiyama, N. Murata. 1985. Evidence that a chlorophyll a' dimer constitutes the photochemical reaction centre 1 (P700) in photosynthetic apparatus. FEBS Lett. 191:252-256.
2. Jordan P., P. Fromme, H. T. Witt, O. Klukas, W. Saenger, N. Krauss. 2001. Three-dimensional structure of cyanobacterial photosystem I at 2.5 Å resolution. Nature 411:909-917.
3. Guergova-Kuras M., B. Boudreaux, A. Joliot, P. Joliot, K. Redding. 2001. Evidence for two active branches for electron transfer in photosystem I. Proc. Natl. Acad. Sci. USA 98:4437-4442.
4. Rigby S. E. J., J. H. A. Nugent, P. J. O'Malley. 1994. ENDOR and special triple resonance studies of chlorophyll cation radicals in photosystem 2. Biochemistry 33:10043-10050.
5. Diner B. A., E. Schlodder, P. J. Nixon, W. J. Coleman, F. Rappaport, J. Lavergne, W. F. J. Vermaas, D. A. Chisholm. 2001. Site-directed mutations at D1-His198 and D2-His197 of photosystem II in *Synechocystis* PCC 6803: sites of primary charge separation and cation and triplet stabilization. Biochemistry 40:9265-9281.
6. Breton J., E. Nabedryk, W. Leibl. 1999. FTIR study of the primary electron donor of Photosystem I (P700) revealing delocalization of the charge in $P700^{+}$ and localization of the triplet character in $^{3}P700$. Biochemistry 38:11585-11592.
7. Davis I. H., P. Heathcote, D. J. MacLachlan, M. C. W. Evance. 1993. Modulation analysis of the electron spin echo signals of *in vivo* oxidised primary donor ^{14}N chlorophyll centres in bacterial, P870 and P960, and plant Photosystem I, P700, reaction centres. Biochim. Biophys. Acta 1143:183-189.
8. Kass H., P. Fromme, H. T. Witt, W. Lubitz. 2001. Orientation and electronic structure of the primary donor radical cation P_{700}^{+} in Photosystem I: a single crystals EPR and ENDOR study. J. Phys. Chem B. 105:1225-1239.
9. Webber A. N., W. Lubitz. 2001. P700: the primary electron donor of photosystem I. Biochim. Biophys. Acta 1507:61-79.
10. Saito K., T. Ishida, M. Sugiura, K. Kawakami, Y. Umena, N. Kamiya, J. R. Shen, H. Ishikita. 2011. Distribution of the cationic state over the chlorophyll pair of photosystem II reaction center. J. Am. Chem. Soc. 133: 14379-14388.
11. Umena Y., K. Kawakami, J.-R. Shen, N. Kamiya. 2011. Crystal structure of oxygen-evolving photosystem II at 1.9 Å resolution. Nature 473:55-60.
12. Brooks B. R., R. E. Bruccoleri, B. D. Olafson, D. J. States, S. Swaminathan, M. Karplus. 1983. CHARMM: a program for macromolecular energy minimization and dynamics calculations. J. Comput. Chem. 4:187-217.
13. MacKerell A. D., Jr., D. Bashford, R. L. Bellott, R. L. Dunbrack, Jr., J. D. Evanseck, M. J. Field, S. Fischer, J. Gao, H. Guo, S. Ha and others. 1998. All-atom empirical potential for molecular modeling and dynamics studies of proteins. J. Phys. Chem. B 102:3586-3616.
14. Rabenstein B., G. M. Ullmann, E.-W. Knapp. 1998. Calculation of protonation patterns in proteins with structural relaxation and molecular ensembles - application to the photosynthetic reaction center. Eur. Bophys. J. 27:626-637.

15. Ishikita H., E.-W. Knapp. 2003. Redox potential of quinones in both electron transfer branches of photosystem I. J. Biol. Chem. 278:52002-52011.
16. Ishikita H., D. Stehlik, J. H. Golbeck, E.-W. Knapp. 2006. Electrostatic influence of PsaC protein binding to the PsaA/PsaB heterodimer in Photosystem I. Biophys. J. 90:1081-1089.
17. Karyagina I., Y. Pushkar, D. Stehlik, A. van der Est, H. Ishikita, E. W. Knapp, B. Jagannathan, R. Agalarov, J. H. Golbeck. 2007. Contributions of the protein environment to the midpoint potentials of the A1 phylloquinones and the Fx iron-sulfur cluster in photosystem I. Biochemistry 46:10804-16.
18. Bayly C. I., P. Cieplak, W. D. Cornell, P. A. Kollman. 1993. A well-behaved electrostatic potential based method using charge restraints for deriving atomic charges: the RESP model. J. Phys. Chem. 97:10269-10280.
19. Jaguar, version 7.5, Schrödinger, LLC, New York, NY, 2008.
20. Bashford D., M. Karplus. 1990. pK_a's of ionizable groups in proteins: atomic detail from a continuum electrostatic model. Biochemistry 29:10219-10225.
21. Ishikita H., W. Saenger, J. Biesiadka, B. Loll, E.-W. Knapp. 2006. How photosynthetic reaction centers control oxidation power in chlorophyll pairs P680, P700 and P870. Proc. Natl. Acad. Sci. USA 103:9855-9860.
22. Ishikita H., J. Biesiadka, B. Loll, W. Saenger, E. W. Knapp. 2006. Cationic state of accessory chlorophyll and electron transfer through pheophytin to plastoquinone in photosystem II. Angew. Chem. Int. Ed. Engl. 45:1964-1965.
23. Rabenstein B., E. W. Knapp. 2001. Calculated pH-dependent population and protonation of carbon-monoxy-myoglobin conformers. Biophys J 80:1141-1150.
24. QSite, version 5.6, Schrödinger, LLC, New York, NY, 2010.
25. Plato M., N. Krauss, P. Fromme, W. Lubitz. 2003. Molecular orbital study of the primary electron donor P700 of photosystem I based on a recent X-ray single crystal structure analysis. Chem. Phys. 294:483-499.
26. Okubo T., T. Tomo, M. Sugiura, T. Noguchi. 2007. Perturbation of the structure of P680 and the charge distribution on its radical cation in isolated reaction center complexes of photosystem II as revealed by fourier transform infrared spectroscopy. Biochemistry 46:4390-4397.
27. Witt H., E. Schlodder, C. Teutloff, J. Niklas, E. Bordignon, D. Carbonera, S. Kohler, A. Labahn, W. Lubitz. 2002. Hydrogen bonding to P700: site-directed mutagenesis of threonine A739 of photosystem I in *Chlamydomonas reinhardtii*. Biochemistry 41:8557-8569.
28. Li Y., M.-G. Lucas, T. Konovalova, B. Abbott, F. MacMillan, A. Petrenko, V. Sivakumar, R. Wang, G. Hastings, F. Gu and others. 2004. Mutation of the putative hydrogen-bond donor to P_{700} of photosystem I. Biochemistry 43:12634-12647.
29. Hastings G., V. M. Ramesh, R. Wang, V. Sivakumar, A. Webber. 2001. Primary donor photo-oxidation in photosystem I: a re-evaluation of ($P700^+$ - P700) Fourier transform infrared difference spectra. Biochemistry 40:12943-9.
30. Nakamura A., T. Suzawa, Y. Kato, T. Watanabe. 2011. Species dependence of the redox potential of the primary electron donor P700 in photosystem I of oxygenic photosynthetic organisms revealed by

spectroelectrochemistry. Plant Cell Physiol 52:815-823.

31. Higgins D. G., J. D. Thompson, T. J. Gibson. 1996. Using CLUSTAL for multiple sequence alignments. Methods Enzymol. 266:383-402.

32. Ishikita H., B. Loll, J. Biesiadka, A. Galstyan, W. Saenger, E.-W. Knapp. 2005. Tuning electron transfer by ester-group of chlorophylls in bacterial photosynthetic reaction center. FEBS Lett. 579:712-716.

ACKNOWLEDGEMENTS

* We are grateful to Dr. Wolfram Saenger and Dr. Ernst-Walter Knapp for useful discussions. This research was supported by the JST PRESTO program (H.I), Grant-in-Aid (21770163 to H.I. and 22740276 to K.S.) for Science Research from the Ministry of Education, Science, Sport and Culture of Japan, Special Coordination Fund (H.I) for Promoting Science and Technology of MEXT, Takeda Science Foundation (H.I.), and Kyoto University Step-up Grant-in-Aid for young scientists (H. I.).

The abbreviations used are:

A_{-1A}/A_{-1B} , accessory Chl*a* in PsaA/PsaB;

Chl*a*, chlorophyll *a*;

Chl*a'*, the $C13^2$ epimer of Chl*a*;

ΔE_m, E_m difference $E_m(P_A) - E_m(P_B)$;

E_m, redox (midpoint) potential;

P_A/P_B, Chl*a'*/Chl*a* molecules that form the P700 heterodimer;

PSI, photosystem I;

PSII, photosystem II;

P700, P_A/P_B (Chl*a'*/Chl*a*) heterodimer;

Table 1. (a) Values of $E_m(P_A)$, $E_m(P_B)$ (in mV), $P_A^{\bullet+}/P_B^{\bullet+}$ ratios, and spin-density distributions in the PSI protein (in %). Δ stands for deletion of atomic charges of the residues/groups.

		***E*m shift (versus reference)[a]**		**Charge**		**Spin**	
(factor)		**P_A**	**P_B**	**$P_A^{\bullet+}$**	**$P_B^{\bullet+}$**	**P_A**	**P_B**
	Wild type	29 [a]	27	27.9	72.1	22.4	77.6
	[H-bond]						
(1)	T743V	20 [a]	28	32.2	67.8	26.9	73.1
	[Epimer]						
(2)	CH_3COO- deleted			32.2	67.8	29.7	70.3
	[PsaA/PsaB pair]						
(3)	Δ(Arg-A750/Ser-B734)			30.6	69.4	25.0	75.0
	[Cofactor]						
(4)	$\Delta(A_{-1A}/A_{-1B})$			24.0	76.0	18.7	81.3

[a] Because E_m(Chl*a*′) in the reference model system is unknown, only the $E_m(P_A)$ shift was calculated. An actual E_m(Chl*a*′) may be higher than E_m(Chl*a*) because Chl*a*′ is thermodynamically less stable than Chl*a* (*9*).

(b) Values of $P_A^{\bullet+}/P_B^{\bullet+}$ ratios and spin-density distributions in vacuum (in %).

	Charge		**Spin**	
	$P_A^{\bullet+}$	**$P_B^{\bullet+}$**	**P_A**	**P_B**
Wild type	41.5	58.5	38.1	61.9
CH_3COO- deleted	45.5	54.5	46.2	53.8

(c) Analysis of factors (listed in Table 1a) that differentiate the populations of $P_A^{\bullet+}$ and $P_B^{\bullet+}$ in the PSI protein environment (in %). Factors (1) T743V (deletion of a H-bond with P_A), (2) CH_3COO- substitution with –H (deletion of the Chl*a*′/Chl*a* difference), and (3) deletion of charges of PsaA/PsaB residue pairs responsible for the $E_m(P_A)/E_m(P_B)$ difference.

Factors	**Charge**		**Spin**	
	$P_A^{\bullet+}$	**$P_B^{\bullet+}$**	**P_A**	**P_B**
Wild type	27.9	72.1	22.4	77.6
(1) + (2)	37.0	63.0	35.1	64.9
(1) + (3)	35.6	64.4	30.5	69.5
(1) + (2) + (3)	40.5	59.5	39.1	60.9

Table 2. Residues that shift $E_m(P_A)$ and $E_m(P_B)$ in the PSI protein environment (mV).

(a) increasing $E_m(P_A)$ and $E_m(P_B)$.

$E_m(P_A)$ shift				$E_m(P_B)$ shift			
	side. [a]	**b.b.** [b]	**Total**		**side.** [a]	**b.b.** [b]	**Total**
Arg-A750	53	12	65	Arg-A651	60	-5	55
Arg-A651	42	-7	35	Arg-A750	30	5	36
Arg-A728	39	-4	35	Arg-A466	32	4	35
Arg-B627	36	-3	33	Arg-B712	36	-4	32
Arg-B712	34	-3	31	Arg-A728	35	-2	32

(b) decreasing $E_m(P_A)$ and $E_m(P_B)$.

$E_m(P_A)$ shift				$E_m(P_B)$ shift			
	side. [a]	**b.b.** [b]	**Total**		**side.** [a]	**b.b.** [b]	**Total**
Asp-B444	-94	4	-90	Asp-A463	-102	4	-98
Asp-A463	-70	3	-67	His-B660	-70	6	-64
His-A680	-72	5	-67	Asp-B444	-66	3	-63
A_{-1A}			-65	F_X			-47
F_X			-48	Asp-B575	-42	0	-42
Asp-B575	-41	0	-42	A_{-1B}			-41
Asp-A593	-33	-2	-35	Asp-B580	-31	-2	-33
His-B660	-31	0	-31	His-A680	-31	-1	-32
Asp-B580	-28	-2	-30	Asp-A593	-29	-2	-31

[a] side. = side chain, [b] b.b. = backbone.

Table 3. PsaA/PsaB residue pairs responsible for ΔE_m (= $E_m(P_A) - E_m(P_B)$, see Figure 2) (mV). Contribution to ΔE_m was obtained as [influence of PsaA on $E_m(P_A)$] + [influence of PsaB on $E_m(P_A)$] – [influence of PsaA on $E_m(P_B)$] – [influence of PsaB on $E_m(P_B)$]. PsaA/PsaB residue pairs in each line were generated from the protein sequence alignment performed with the CLUSTAL program (*31*) (Figure 4).

(a) ΔE_m increasing pairs (i.e., pairs that contribute to accumulation of $P_B^{\bullet+}$).

PsaA			PsaB			
	$E_m(P_A)$	$E_m(P_B)$		$E_m(P_A)$	$E_m(P_B)$	ΔE_m
Arg-A750	65	36	Ser-B734	9	21	17
--	--	--	Asp-B92	-15	-24	9

(b) ΔE_m decreasing pairs (i.e., pairs that contribute to accumulation of $P_A^{\bullet+}$).

PsaA			PsaB			
	$E_m(P_A)$	$E_m(P_B)$		$E_m(P_A)$	$E_m(P_B)$	ΔE_m
A_{-1A}	-65	-23	A_{-1B}	-19	-41	–28
Gln-A657	-4	-2	Asn-B633	18	26	-14

Table 4. Influence of the orientation of the methyl-ester group of A_{-1A}/A_{-1B} on the $P_A^{\bullet+}/P_B^{\bullet+}$ ratio and spin-density distribution calculated in the PSI protein (in %).

	Charge		**Spin**	
	$P_A^{\bullet+}$	**$P_B^{\bullet+}$**	**P_A**	**P_B**
Wild type	**27.9**	**72.1**	**22.4**	**77.6**
[Rotated methyl-ester]				
A_{-1A}	26.6	73.4	19.7	80.3
A_{-1B}	23.5	76.5	17.4	82.6
A_{-1A}/A_{-1B}	**22.4**	**77.6**	**15.1**	**84.9**

FIGURE LEGENDS

FIGURE 1. (a) Geometry of Chl*a* (R1 = CH_3COO-, R2= H) and the $C13^2$ epimer, Chl*a′* (R1 = H, R2 = CH_3COO-). (b) E_m values of Chl*a* and Chl*a′* in the reference system (e.g., aprotic solvents).

FIGURE 2. Relationship between E_m and population of the cationic state over the P_A/P_B pair. The + sign indicates a population of the energetically distributed cationic state owing to the E_m levels. $\Delta E_m = E_m(P_A) - E_m(P_B)$.

FIGURE 3. Arrangement of residues in PsaA/PsaB of PSI. Side chains of basic and acidic residues are depicted as blue and red sticks, respectively. (a) Residues increasing $E_m(P_A)$ or $E_m(P_B)$. (b) Residues decreasing $E_m(P_A)$ or $E_m(P_B)$. (c) Residue pairs enhancing $E_m(P_A) > E_m(P_B)$. (d) All acidic and basic residues in PsaA/PsaB.

FIGURE 4. Amino acid sequences of the PsaA and PsaB subunits of PSI from *T. elongatus*, *Synechocystis* PCC 6803 (S.6803), *Chlamydomonas reinhardtii* (C. reinhardtii), and spinach. PsaA/PsaB residue pairs in each line were generated from the protein sequence alignment performed with the CLUSTAL program (*31*).

FIGURE 5. Geometry of the accessory Chl*a* A_{-1A} and A_{-1B}. The solid and dotted lines indicate the distances between the Mg atom and the O atoms of the carbonyl and ester groups, respectively.

(a)

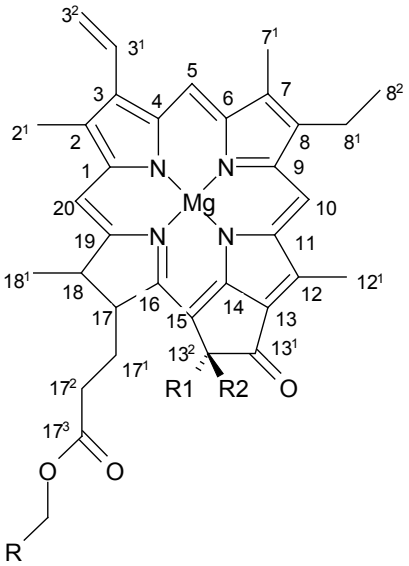

(b)

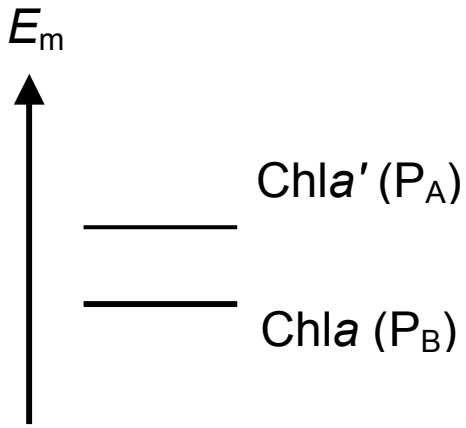

Figure 1.

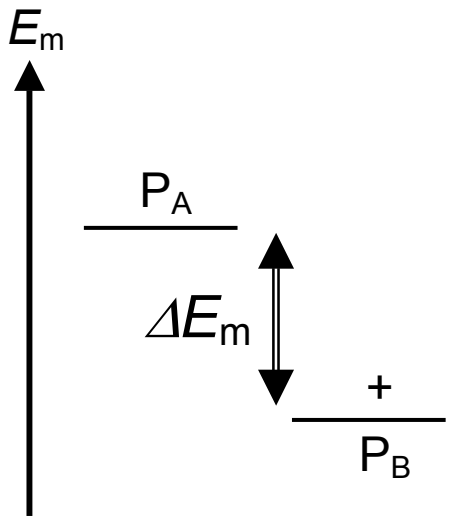

Figure 2.

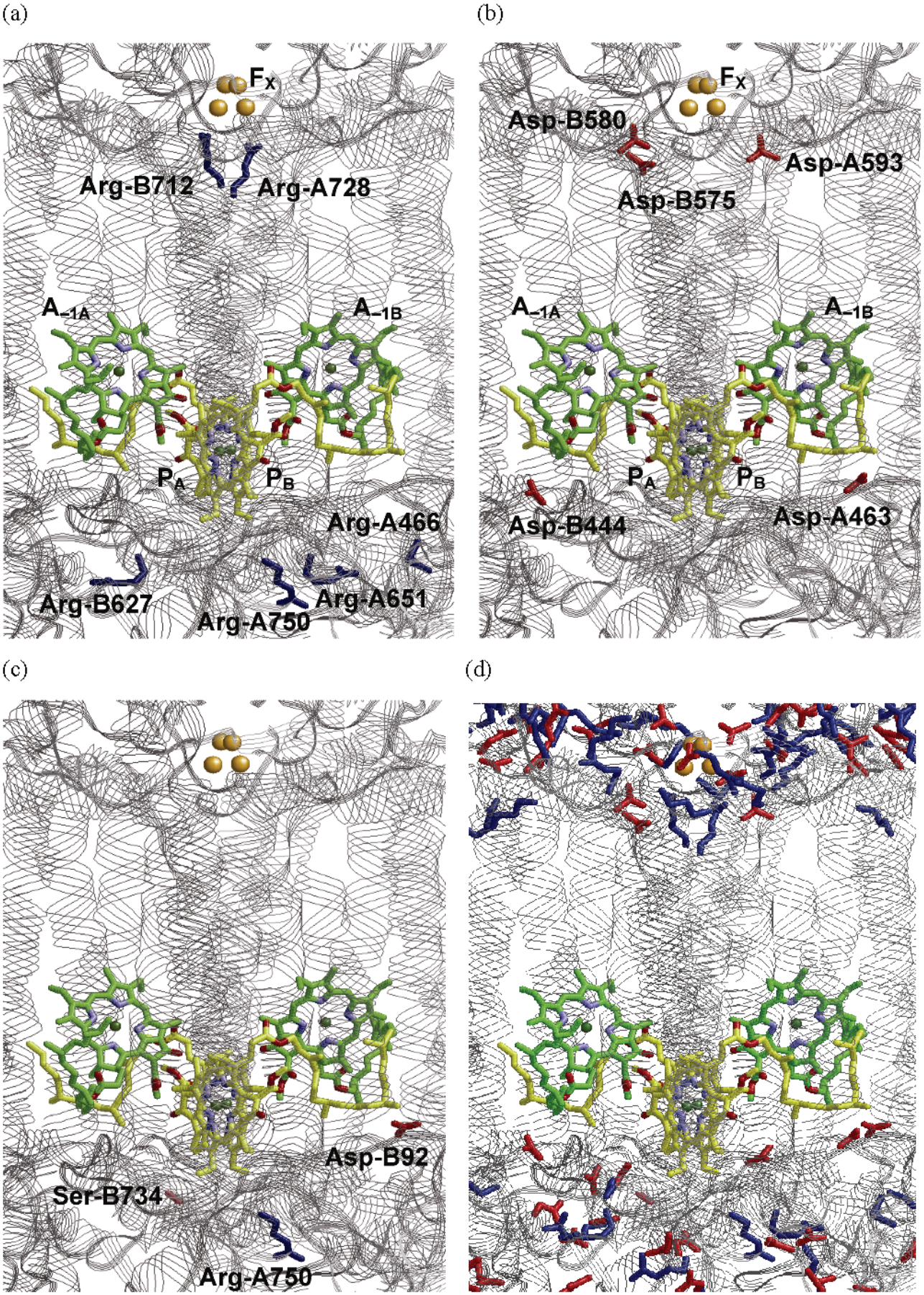

Figure 3.

```
                      98          108         118         127         137
PsaA T.elongatus      SNYEAWLADP TGIKPSAQVV W-PIVGQGIL NGDVGGGFHG -IQIT-SGLF
PsaA S.6803           SNYEGWLADP THIKPSAQVV W-PIVGQGIL NGDVGGGFHG -IQIT-SGLF
PsaA C.reinhardtii    SNYEAWLSDP THIKPSAQVV W-PIVGQEIL NGDVGGGFQG -IQIT-SGFF
PsaA spinach          SNYEAWLSDP THIGPSAQVV W-PIVGQEIL NGDVGGGFRG -IQIT-SGFF
                      71          81          91          101         111
PsaB T.elongatus      GNFEQWVQDP VNTRPIAHAI WDPQFGKAAV DAFTQAGASN PVDIAYSGVY
PsaB S.6803           GNFEQWIKDP LNIRPIAHAI WDPHFGEGAV NAFTQAGASN PVNIAYSGVY
PsaB C.reinhardtii    GNFEQWVTDP VHIRPIAHAI WDPHFGQPAV EAFTRGGASG PVNISTSGVY
PsaB spinach          GNFESWVQDP LHVRPIAHAI WDPHFGQPAV EAFTRGGALG PVNIAYSGVY

                      711         718         727         737         747
PsaA T.elongatus      LKVAPAI--- -QPRALSIIQ GRAVGVAHYL LGGIATTWAF FLARIISVG-
PsaA S.6803           LNVAPAI--- -QPRALSIIQ GRAVGVAHYL LGGIVTTWAF FLARSLSIG-
PsaA C.reinhardtii    LKVAPAI--- -QPRALSITQ GRAVGVAHYL LGGIATTWSF FLARIISVG-
PsaA spinach          LKVAPAT--- -QPRALSIVQ GRAVGVTHYL LGGIATTWAF FLARIIAVG-
                      691         701         711         721         731
PsaB T.elongatus      TPLANLVRWK DKPVALSIVQ ARLVGLAHFS VGYILTYAAF LIASTAAKFG
PsaB S.6803           TPLANLVRWK DKPVALSIVQ ARLVGLAHFT VGYVLTYAAF LIASTAGKFG
PsaB C.reinhardtii    TPLANLVYWK DKPVALSIVQ ARLVGLAHFS VGYIFTYAAF LIASTSGRFG
PsaB spinach          TPLANLIRWR DKPVALSIVQ ARLVGLAHFS VGYIFTYAAF LIASTSGKFG
```

Figure 4.

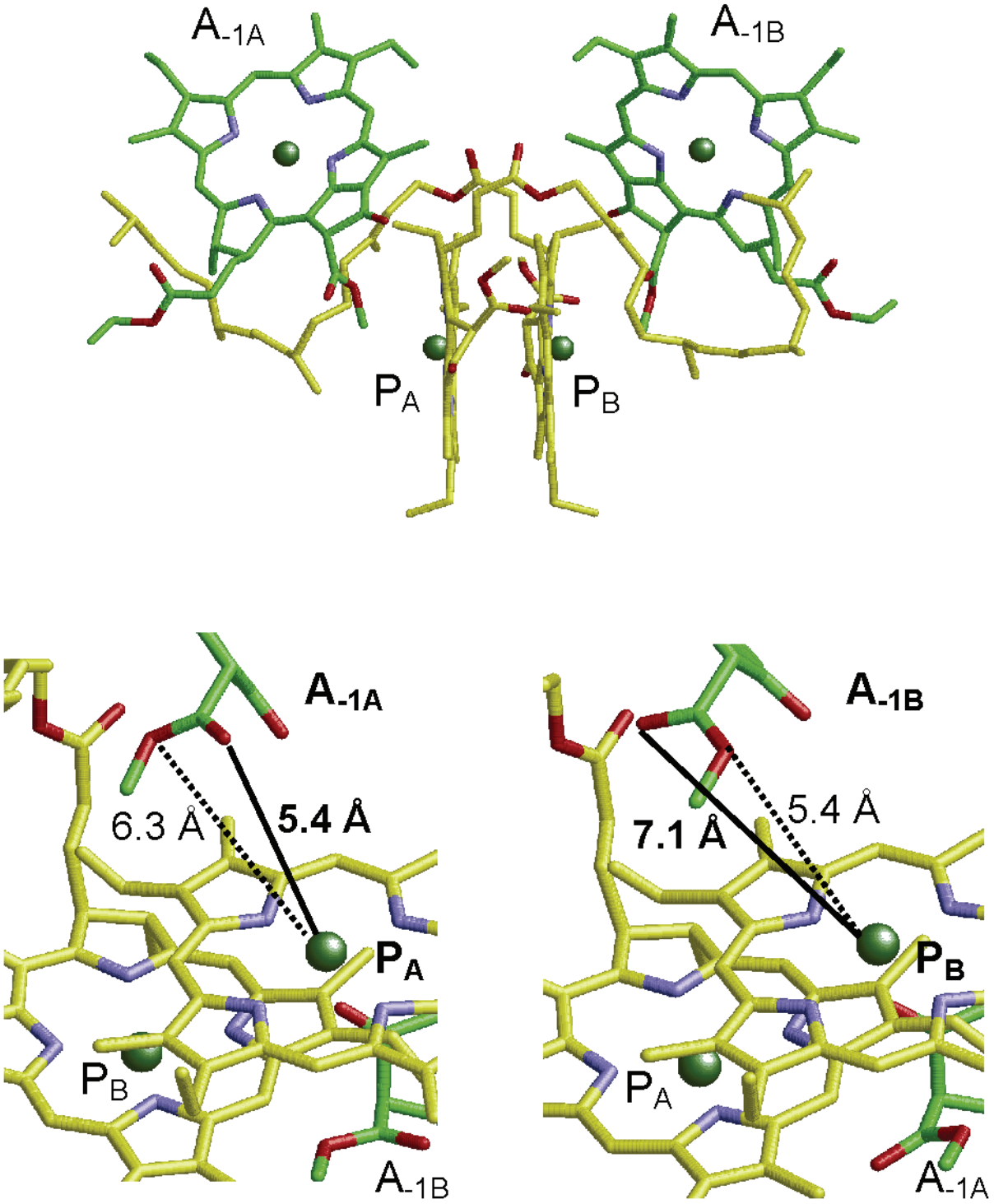

Figure 5.